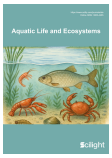
Scilight

Aquatic Life and Ecosystems
https://www.sciltp.com/journals/ale



Check for updates

Article

Comparative Growth Kinetics, Hydrocarbon Accumulation, and Isomeric Distribution across Three Chemical Races of *Botryococcus braunii*

Huijun Xu [1] and Liang Song [2,3,*]

[1] Southern Marine Science and Engineering Guangdong Laboratory (Guangzhou), 1119 Nansha Street, Nansha, Guangzhou 511458, China
[2] College of Science and Engineering, Flinders University, Adelaide GPO Box 2100, SA, Australia
[3] State Key Laboratory of Marine Food Processing & Safety Control, National Engineering Research Center of Seafood, School of Food Science and Technology, Dalian Polytechnic University, Dalian 116034, China
* Correspondence: ryo.song@foxmail.com

How To Cite: Xu, H.; Song, L. Comparative Growth Kinetics, Hydrocarbon Accumulation, and Isomeric Distribution across Three Chemical Races of *Botryococcus braunii*. *Aquatic Life and Ecosystems* **2026**, *2*(4), 17. https://doi.org/10.53941/ale.2026.100017

Received: 7 September 2026
Revised: 22 October 2026
Accepted: 2 November 2026
Published: 12 November 2026

Abstract: This comparative study evaluated biomass growth kinetics, hydrocarbon accumulation dynamics, and compositional signatures across three representative *Botryococcus braunii* chemical races, namely UTEX 572 (Race A), Ayamè (Race B), and Madras 3 (Race L), over a 42-day batch cultivation period. Growth trajectories revealed differing strain-specific kinetics. Specifically, Specifically, UTEX 572 completed its exponential phase rapidly from days 3 to 12, whereas Ayamè and Madras 3 required an extended initial acclimation period before initiating active growth phase from day 12 to day 30. During exponential growth, UTEX 572 achieved a maximum specific growth rate of 0.168 ± 0.008 day^{-1} and a peak volumetric productivity of 0.029 ± 0.001 g L^{-1} day^{-1}, significantly exceeding Ayamè and Madras 3. Conversely, Ayamè attained a peak hydrocarbon content of 27.2 ± 1.4% and a final yield of 0.466 g L^{-1} upon entering the stationary phase. Gas chromatography-mass spectrometry confirmed that signature homologous series distributions remained stable across all growth phases, despite subtle temporal isomeric shifts. Crucially, these performance patter represent strain-specific acclimation constrained strictly by the standardized baseline framework, Bold-3N medium at 24 °C, rather than defining absolute limits on intrinsic biological potential. These findings demonstrate a physiological trade-off between rapid population turnover and storage accumulation under unified baseline conditions. Consequently, UTEX 572 serves as an efficient candidate for short-cycle harvesting systems, whereas higher-accumulating strains like Ayamè represent valuable targets for extended extraction strategies pending further environmental optimization.

Keywords: *Botryococcus braunii*; growth kinetics; hydrocarbon accumulation; isomeric distribution; baseline regime constraints; biofuel feedstock

1. Introduction

The global transition toward sustainable energy has driven extensive research into biofuels as an environmentally sound alternative to fossil fuels [1]. Commercial biodiesel relies heavily on transesterification of vegetable oils and animal tallow derived from conventional agricultural crops, including rapeseed, soybean, sunflower, and palm [2]. However, the utilization of arable land for feedstock production intensifies the critical food-versus-fuel conflict [3]. Microalgae have emerged as a promising alternative feedstock because they exhibit

Copyright: © 2026 by the authors. This is an open access article under the terms and conditions of the Creative Commons Attribution (CC BY) license (https://creativecommons.org/licenses/by/4.0/).
Publisher's Note: Scilight stays neutral with regard to jurisdictional claims in published maps and institutional affiliations.

significantly higher growth rates and lipid productivity than traditional oil-seed crops, occasionally yielding up to an order of magnitude higher lipid production per unit area [4].

Among various microalgal candidates, the colonial green alga *Botryococcus braunii* has attracted considerable interest due to its capacity for autotrophic growth [5] and the abundant synthesis of hydrocarbon molecules, which are uniquely secreted and sequestered within the extracellular colony matrix [6]. These unique physiological traits position *B. braunii* as a promising biological platform for renewable hydrocarbon production [7]. Despite its high potential, large-scale commercialization remains economically unviable [8], largely due to substantial phenotypic and metabolic variability across divergent strains [9]. Previous investigations demonstrate that hydrocarbon yield is heavily modulated by environmental parameters, such as nutrient availability [10,11], light regimes [12,13], photobioreactor design [14,15] and sulfur-containing compounds [16]. Consequently, systematically evaluating algal growth kinetics and hydrocarbon productivity across heterogeneous strains under identical culture conditions provides a fundamental baseline to benchmark relative strain performance.

Although previous comparative efforts have examined *B. braunii* performance under varying physical stimuli [17], an incomplete understanding persists regarding the metabolic shifts occurring across various algal growth phases. In other microalgal taxa like *Thalassiosira pseudonana* [18], *Isochrysis galbana* [19], *Gymnodinium* sp. [20], and *Nannochloropsis oculata* [21], lipid and triacylglycerol profiles fluctuate dynamically throughout the growth cycle, primarily driven by the redirection of carbon flux from cellular proliferation pathways to energy storage mechanisms upon nutrient depletion [22]. Although hydrocarbon productivity in *B. braunii* is known to peak during active cell division [23], a comprehensive understanding of how biomass accumulation, volumetric productivity, and internal hydrocarbon isomeric distribution co-evolve synchronously across all major growth phases, including lag, exponential, stationary, and decline phases, remains inadequately established.

Furthermore, *B. braunii* exhibits pronounced morphological and chemical heterogeneity, and it is categorized phylogenetically and chemically into three discrete chemical races, designated as Race A, Race B, and Race L based on a combination of 18S rRNA phylogenetic analysis and signature hydrocarbon profiling [24]. These chemical races reflect fundamentally divergent metabolic origins and biosynthetic pathways [25]. Race A synthesizes odd-numbered C_{25} to C_{31} n-alkadienes and alkatrienes derived from modified fatty acid elongation and reduction pathways. In contrast, Race B produces C_{30} to C_{37} branched triterpene botryococcenes via the cytosolic mevalonate pathway, whereas Race L is predominantly characterized by the synthesis of the C_{40} tetraterpene lycopadiene generated through the plastidial methylerythritol phosphate pathway. Crucially, the specific chain lengths and molecular structures synthesized by Race A and Race B serve as promising chemical feedstocks for hydrocracking into drop-in aviation and diesel fuels [26]. However, previous comparative studies have been strictly confined within single chemical races or isolated sampling timepoints, leaving comprehensive inter-race evaluations of hydrocarbon compositional dynamics throughout full batch cultivation cycles largely unexplored.

Motivated by these uncharacterized metabolic dynamics, this study investigates one representative strain from each chemical race, specifically *B. braunii* UTEX 572 for Race A, *B. braunii* Ayamè for Race B, and *B. braunii* Madras 3 for Race L. Herein, biomass accumulation, hydrocarbon content, and specific productivity are systematically examined throughout defined growth phases for all three evaluated strains under a standardized batch cultivation framework. While applying a uniform liquid medium, specifically Bold-3N, and a constant temperature of 24 °C is methodologically necessary to establish a direct comparative baseline, it is recognized that these standardized parameters inevitably impose varying degrees of environmental sub-optimality across geographically and phylogenetically disparate isolates. Consequently, the observed kinetic disparities, including the extended acclimation phases in Ayamè and Madras 3, represent strain-specific performance governed by the present cultivation framework rather than defining absolute biological limits. By elucidating how hydrocarbon quantity and quality evolve across developmental stages, this work provides a quantitative framework for evaluating the inherent trade-offs among biomass growth rate, hydrocarbon content, and overall productivity, thereby offering robust criteria for industrial strain selection in biofuel engineering while underscoring the critical necessity for future race-specific nutritional optimization.

2. Materials and Methods

2.1. Algal Strains and Cultivation

Three *Botryococcus* strains from divergent geographic origins were evaluated. The UTEX 572 strain was obtained from the University of Texas Culture Collection (USA), whereas strains Ayamè and Madras 3 were acquired from the National Centre of Scientific Research (France). Batch cultures were maintained for 42 days in 250 mL Erlenmeyer flasks containing 120 mL of liquid Bold-3N medium, with initial biomass density adjusted to approximately 0.35 g L^{-1} upon inoculation. Cultures were incubated at 24 ± 1 °C under a constant photon flux

density of 150 μmol s^{-1} m^{-2} with a 12-h light/dark photoperiod. To establish a standardized low-shear baseline for comparative physiological evaluation while preventing wall-growth adherence, flasks were manually agitated twice daily. Because *Botryococcus braunii* forms delicate extracellular colonial matrices rich in long-chain hydrocarbons, the organism is highly sensitive to hydrodynamic shear stress, where continuous mechanical shaking can disrupt colonial integrity. Consequently, this standardized low-shear baseline mode was deliberately chosen to isolate intrinsic racial growth kinetics under uniform hydrodynamic constraints, ensuring that comparative evaluations among strains remained unbiased by mechanical disruption. Sampling was performed on days 0, 3, 6, 12, 18, 24, 30, 36, and 42 to assess biomass accumulation and hydrocarbon dynamics. All experimental trials were conducted in biological triplicate under identical protocols.

2.2. Growth Phase Characterization

Biomass quantification was performed by filtering culture aliquots through pre-weighed membrane filters, rinsing cells with distilled water, and determining dry weight via freeze-drying followed by gravimetric measurement, expressed as g L^{-1} [27]. Growth kinetics were evaluated over defined developmental intervals. Standard batch culture models define recognized physiological phases; herein, quantitative tracking focused on four primary intervals, namely lag, exponential, stationary, and decline phases. While comprehensive biological kinetic tracking spanned the full 42-day cultivation cycle for all strains, including the 12-day decline phase observed in UTEX 572 from day 30 to day 42, downstream specific yield calculations were strictly standardized to the primary growth phases to maintain physiological comparability across strains. The lag phase represented the initial acclimation period following inoculation, and the exponential phase was defined by logarithmic cell density increase over time. The stationary phase corresponded to the period when nutrient limitation and growth rate reached equilibrium, resulting in a stable biomass density. The decline phase marked a reduction in cell density and culture viability.

2.3. Hydrocarbon Extraction and Quantification

Hydrocarbon extraction was executed on freeze-dried biomass via solvent extraction using *n*-hexane coupled with cell disruption by ultrasonication. Suspensions were centrifuged at 1000× *g* for 10 min at 15 °C, and supernatants were collected repeatedly until visually colorless. Combined supernatants were fractionated via alumina column chromatography, isolating the hydrocarbon fraction prior to the carotene elution band. Solvent was evaporated under a continuous nitrogen stream, and hydrocarbon content was quantified gravimetrically as a percentage of dry weight.

2.4. Calculation of Specific Growth Rate and Specific Hydrocarbon Productivity

The specific mass growth rate (μ, day^{-1}) during the exponential phase was determined from the biomass increase between the initial and final sampling dates of the exponential interval. The specific growth rate (μ) was calculated using the equation $\mu = \mathrm{Ln}\,(M_2 / M_1) / (t_2 - t_1)$, where M_1 and M_2 denote the biomass concentration (g L^{-1}) at time 1 (t_1) and time 2 (t_2), respectively [28]. Similarly, the specific hydrocarbon productivity (P, g L^{-1} day^{-1}) during the exponential phase was calculated using the equation $P = (H_2 - H_1) / (t_2 - t_1)$, where H_1 and H_2 represent the volumetric hydrocarbon concentration (g L^{-1}) at time 1 (t_1) and time 2 (t_2), respectively [29].

2.5. Hydrocarbon Analysis

Hydrocarbons were separated by gas chromatography (GC) and identified by gas chromatography-mass spectrometry (GC-MS) using an Agilent Technologies 5975C mass spectrometer coupled with a 7890A gas chromatograph and a 7683B autosampler. Both GC and GC-MS analyses were performed using an HP-5MS capillary column (or equivalent) measuring 15 m in length, 0.25 mm in inner diameter, and 0.25 μm in film thickness. The oven temperature was initially maintained at 40 °C for 4 min post-injection, subsequently increased to 325 °C at a rate of 20 °C min^{-1}, and held for 10 min, with a carrier gas flow rate of 2 mL min^{-1}. Injector and detector temperatures were maintained at 300 and 325 °C, respectively. Mass spectra were acquired under electron ionisation at 70 eV over a mass range of 35 to 550 m/z. Hydrocarbon compounds were identified by molecular ion confirmation and mass spectral comparison against the NIST library for LC/MSD via ChemStation software (rev. B.01.03, Agilent Technologies) alongside reference mass spectra from external standards (unpublished data provided by Pierre Metzger, National Centre of Scientific Research, France). Isomeric fractions discussed herein are classified based on chromatographic resolution and standardized retention times (R_t) under the specified GC

parameters, reflecting proportional variations among resolved structural variants rather than absolute stereochemical elucidation.

2.6. Statistical Analysis

All experimental trials were conducted with three independent biological replicates ($n = 3$), and values are presented as means ± standard deviations (SD). Statistical analyses were performed using SPSS 24.0 software. For individual strains, temporal variations in growth parameters, volumetric hydrocarbon yields, and relative isomeric distributions throughout all sampling days were evaluated using one-way analysis of variance (ANOVA). Strain-specific comparisons of kinetic parameters during the active exponential phase and maximum cumulative metrics during the stationary phase were likewise evaluated via one-way ANOVA. Post-hoc evaluations of statistically significant differences were conducted using Tukey's honest significant difference (HSD) test. Differences were considered statistically significant at $p \leq 0.05$.

3. Results

3.1. Algal Biomass

Three *B. braunii* strains were inoculated at an initial density of approximately 0.35 g L^{-1}, and their subsequent growth trajectories exhibited differing kinetics over the 42-day cultivation period ($p < 0.05$, Figure 1). The UTEX 572 strain experienced a 3-day lag phase, immediately followed by an exponential growth period extending from day 3 to day 12. After an 18-day stationary phase, this strain entered a decline phase starting on day 30. In contrast, constrained by the standardized baseline conditions applied herein, specifically Bold-3N medium at 24 °C, the Ayamè and Madras 3 strains both required an initial 12-day acclimation period before initiating their 18-day exponential phases from day 12 to day 30. Neither of these two strains exhibited a decline phase, maintaining stable biomass densities through the end of the experiment. During the exponential phase, the specific growth rate of UTEX 572 was 0.168 ± 0.008 day^{-1}, which was significantly higher than those of Ayamè at 0.076 ± 0.002 day^{-1} and Madras 3 at 0.075 ± 0.003 day^{-1} ($p < 0.05$, Figure 2), with no statistical difference observed between the latter two. Consequently, maximum biomass concentrations differed significantly among the evaluated races ($p < 0.05$, Figure 3). UTEX 572 produced the highest biomass yield of 1.83 ± 0.041 g L^{-1}, followed by Ayamè at 1.72 ± 0.260 g L^{-1}, while Madras 3 exhibited the lowest accumulation capability reaching 1.39 ± 0.007 g L^{-1}.

3.2. Hydrocarbon Content and Yield

Cellular and matrix-associated hydrocarbon contents across all *B. braunii* strains varied dynamically in a phase-dependent manner ($p < 0.05$, Figure 1). The hydrocarbon content of the UTEX 572 strain increased rapidly by 1.65-fold during active growth, peaking at 16.8 ± 0.8% on a dry weight basis on day 12, but decreased to approximately 13.0% by day 30 ($p < 0.05$). Conversely, Ayamè and Madras 3 demonstrated continuous hydrocarbon accumulation well into the stationary phase. Ayamè reached its maximal content of 27.2 ± 1.4% on day 30, while Madras 3 peaked at 7.1 ± 0.2% on day 36.

Driven by the combined dynamics of biomass and cellular content, the volumetric hydrocarbon yields varied significantly over time ($p < 0.05$, Table 1). Volumetric yields consistently increased from the lag phase through the exponential phase in all strains, subsequently plateauing or declining upon entering the stationary phase. UTEX 572 achieved its maximum yield of 0.303 g L^{-1} on day 18. Ayamè reached the absolute highest yield of 0.466 g L^{-1} on day 42, whereas Madras 3 plateaued at 0.099 g L^{-1} from day 36 onwards. Despite having a lower final yield than Ayamè, kinetic analysis during the active exponential phase revealed that UTEX 572 possessed the highest specific hydrocarbon productivity at 0.029 ± 0.001 g L^{-1} day^{-1}, significantly exceeding both Ayamè at 0.023 ± 0.001 g L^{-1} day^{-1} and Madras 3 at 0.005 ± 0.001 g L^{-1} day^{-1} ($p < 0.05$, Figure 2). Overall, regarding maximum accumulation capacity during the entire cultivation, Ayamè was statistically higher than UTEX 572, which in turn was significantly higher than Madras 3 ($p < 0.05$, Figure 3).

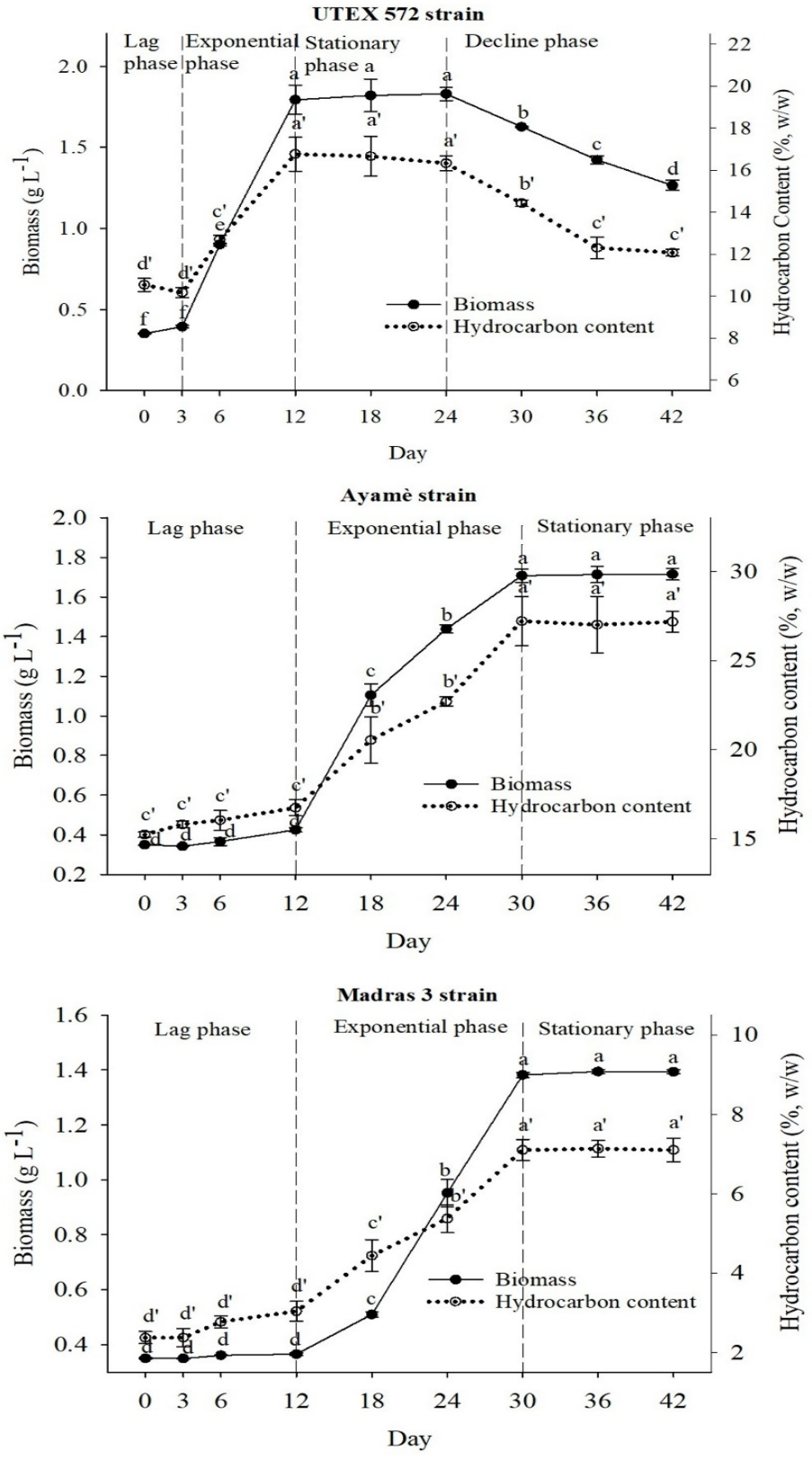


Figure 1. Growth kinetics and temporal hydrocarbon accumulation profiles of the three *B. braunii* strains (UTEX 572, Ayamè, and Madras 3) over a 42-day batch cultivation. The background colors delineate distinct developmental phases (lag, exponential, stationary, and decline phases) based on biomass accumulation patterns. Data are presented as mean ± standard error ($n = 3$). Different lowercase letters (a, b, c, etc., for biomass; a', b', c', etc., for hydrocarbon content) indicate statistically significant differences between adjacent sampling days for each independent strain at $p \leq 0.05$, according to Tukey's multiple comparisons test.

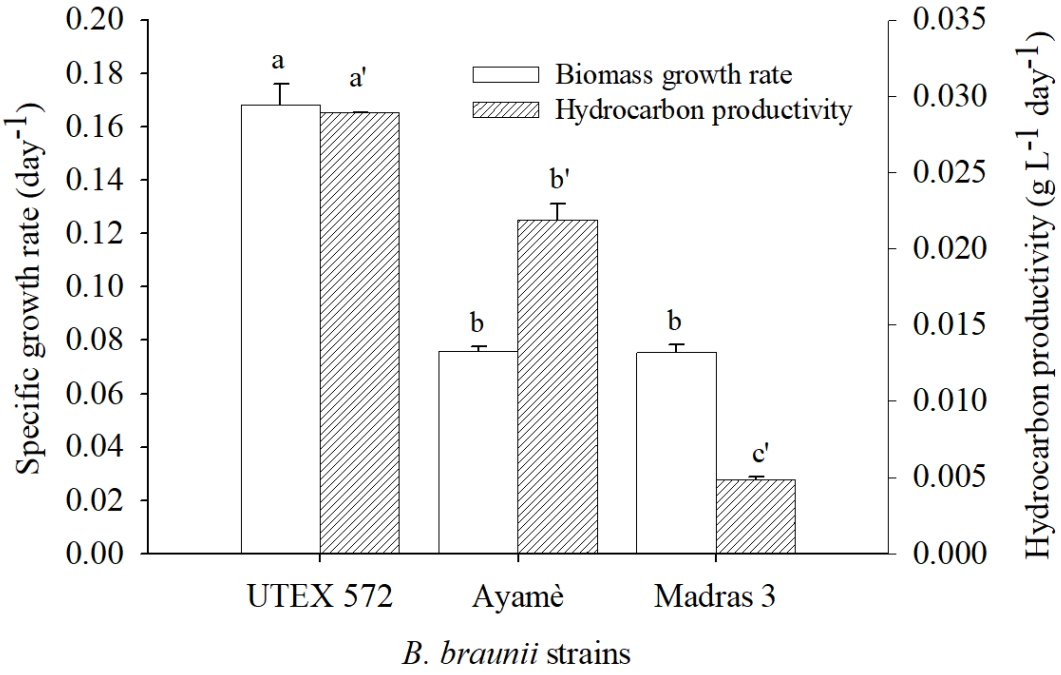


Figure 2. Specific biomass growth rate (day^{-1}) and specific hydrocarbon productivity (g L^{-1} day^{-1}) of the three *B. braunii* strains evaluated during their respective exponential growth phases. Data are presented as mean ± standard error (n = 3). Different lowercase letters (a, b, c for specific growth rate; a', b', c' for specific hydrocarbon productivity) indicate statistically significant differences among the evaluated algal strains at $p \leq 0.05$, according to Tukey's multiple comparisons test.

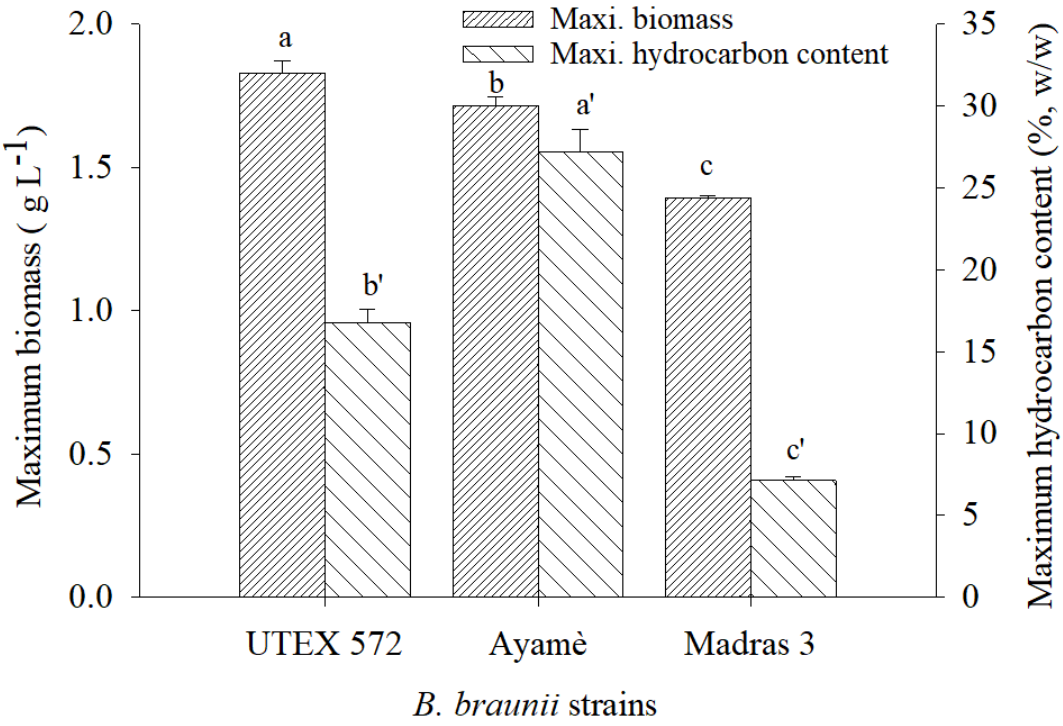


Figure 3. Maximal biomass yield (g L^{-1}) and maximal hydrocarbon content (%, w/w) achieved by the three *B. braunii* strains during the entire 42-day cultivation period. Data are presented as mean ± standard error (n = 3). Different lowercase letters (a, b, c for maximal biomass; a', b', c' for maximal hydrocarbon content) indicate statistically significant differences among the tested algal strains at $p \leq 0.05$, according to Tukey's multiple comparisons test.

Table 1. Temporal variations in volumetric hydrocarbon yield (g L^{-1}) among the three *B. braunii* strains during a 42-day batch cultivation.

B. braunii	**Hydrocarbon Yield (g L^{-1}) on Each Sampling Day**								
Strains	**0**	**3**	**6**	**12**	**18**	**24**	**30**	**36**	**42**
UTEX 572	0.037 ± 0.003 ^{a}	0.040 ± 0.004 ^{a}	0.114 ± 0.008 ^{b}	0.301 ± 0.011 ^{d}	0.303 ± 0.010 ^{d}	0.299 ± 0.014 ^{d}	0.234 ± 0.012 ^{c}	0.175 ± 0.009 ^{b}	0.153 ± 0.008 ^{b}
Ayamè	0.053 ± 0.004 ^{a}	0.054 ± 0.005 ^{a}	0.059 ± 0.005 ^{a}	0.071 ± 0.006 ^{a}	0.226 ± 0.012 ^{b}	0.327 ± 0.011 ^{c}	0.465 ± 0.016 ^{d}	0.462 ± 0.014 ^{d}	0.466 ± 0.016 ^{d}
Madras 3	0.008 ± 0.001 ^{a}	0.008 ± 0.000 ^{a}	0.010 ± 0.000 ^{a}	0.011 ± 0.001 ^{a}	0.023 ± 0.002 ^{b}	0.051 ± 0.004 ^{c}	0.098 ± 0.004 ^{d}	0.099 ± 0.005 ^{d}	0.099 ± 0.003 ^{d}

Note: Values are expressed as mean ± standard deviation (n = 3). Different lowercase superscript letters (a, b, c, d) within the same row indicate statistically significant differences among sampling days for a given strain ($p \leq 0.05$).

3.3. Hydrocarbon Composition and Distribution

Gas chromatography-mass spectrometry (GC-MS) confirmed the specific chemical races of the strains. Representative chromatograms for each race illustrate these characteristic retention time separations and unique elution profiles (Figure S1). Based on standardized chromatographic retention times and mass spectral fragmentation patterns, the UTEX 572 strain representing Race A synthesized hydrocarbons with chain lengths ranging from C_{25} to C_{31}, predominated by C_{29} and C_{31} fractions (Table 2). Four resolvable isomers of both C_{29} and C_{31} were identified based on retention times. The overall carbon chain distribution in UTEX 572 remained highly stable throughout cultivation. However, temporal isomeric tracking revealed a gradual shift in which the relative abundance of the primary isomer C_{29a} (R_t = 17.687 min) steadily increased from 36.0% on day 6 to a peak of 41.5% by day 36, accompanied by a concurrent reduction in minor C_{29} isomers (C_{29b}, C_{29c}, and C_{29d}). The C_{31} and minor C_{25} and C_{27} proportions remained relatively constant.

Table 2. Temporal dynamics of relative hydrocarbon composition (%) in the *B. braunii* UTEX 572 strain (Race A).

Hydrocarbons	**Retention Time (min)**	**Relative Quantity (%) on Each Sampling Day**								
		0	**3**	**6**	**12**	**18**	**24**	**30**	**36**	**42**
C_{25}	16.247	0.64 ± 0.04 ^{a}	0.68 ± 0.01 ^{a}	0.60 ± 0.08 ^{a}	0.63 ± 0.04 ^{a}	0.58 ± 0.07 ^{a}	0.86 ± 0.07 ^{a}	0.72 ± 0.09 ^{a}	0.73 ± 0.01 ^{a}	0.66 ± 0.01 ^{a}
C_{27}	16.993	6.17 ± 0.21 ^{a}	6.71 ± 0.25 ^{a}	6.33 ± 0.40 ^{a}	6.29 ± 0.42 ^{a}	6.94 ± 0.28 ^{a}	6.54 ± 0.73 ^{a}	5.89 ± 0.19 ^{a}	5.44 ± 0.38 ^{a}	6.34 ± 0.52 ^{a}
C_{29a}	17.687	35.98 ± 0.85 ^{a}	35.48 ± 0.79 ^{a}	35.98 ± 0.42 ^{a}	36.94 ± 0.91 ^{ab}	37.60 ± 0.25 ^{b}	40.04 ± 1.12 ^{bc}	40.38 ± 1.05 ^{bc}	41.53 ± 0.95 ^{c}	41.13 ± 0.88 ^{c}
C_{29b}	17.760	3.98 ± 0.15 ^{a}	3.94 ± 0.14 ^{a}	3.95 ± 0.19 ^{a}	3.62 ± 0.02 ^{ab}	3.60 ± 0.43 ^{ab}	3.21 ± 0.21 ^{b}	2.20 ± 0.28 ^{c}	2.33 ± 0.09 ^{c}	2.26 ± 0.38 ^{c}
C_{29c}	17.800	5.80 ± 0.20 ^{a}	5.88 ± 0.22 ^{a}	5.89 ± 0.41 ^{a}	5.95 ± 0.53 ^{a}	4.97 ± 0.38 ^{b}	4.34 ± 0.65 ^{bc}	4.41 ± 0.86 ^{bc}	4.02 ± 0.34 ^{c}	3.73 ± 0.13 ^{c}
C_{29d}	17.900	6.25 ± 0.24 ^{a}	6.46 ± 0.46 ^{a}	5.95 ± 0.22 ^{ab}	5.41 ± 0.39 ^{bc}	5.00 ± 0.17 ^{c}	4.29 ± 0.55 ^{d}	4.02 ± 0.34 ^{d}	3.42 ± 0.02 ^{e}	3.23 ± 0.11 ^{e}
C_{31a}	18.335	39.82 ± 0.92 ^{a}	39.63 ± 0.30 ^{a}	39.82 ± 0.89 ^{a}	39.78 ± 0.43 ^{a}	40.01 ± 0.95 ^{a}	39.45 ± 0.88 ^{a}	41.12 ± 1.02 ^{a}	41.35 ± 1.01 ^{a}	41.44 ± 0.86 ^{a}
C_{31b}	18.455	1.36 ± 0.06 ^{a}	1.22 ± 0.01 ^{a}	1.48 ± 0.07 ^{a}	1.38 ± 0.09 ^{a}	1.30 ± 0.05 ^{a}	1.27 ± 0.08 ^{a}	1.26 ± 0.07 ^{a}	1.18 ± 0.04 ^{a}	1.21 ± 0.01 ^{a}

Note: Values are expressed as mean ± standard deviation (n = 3). Different lowercase superscript letters (a, b, c, d, e) within the same row indicate statistically significant differences among sampling days for a given hydrocarbon fraction ($p \leq 0.05$). Subscripts a, b, c, and d represent isomers of the C_{29} or C_{31} hydrocarbon with different retention times.

For the Ayamè strain (Race B), hydrocarbons were predominantly represented by C_{33} and C_{34}, with C_{34} comprising over 90% of the total fraction (Table 3). While the dominant C_{34} carbon chain length remained constant, its internal isomeric distribution exhibited a pronounced dynamic shift as the culture aged. The predominant isomer, C_{34d} (R_t = 16.279 min), significantly increased from 43.3% at the onset of the exponential phase on day 12 to 54.8% by day 36 in the stationary phase. Consequently, the relative proportions of its associated isomers (C_{34a}, C_{34b}, and C_{34c}) declined concomitantly.

Table 3. Temporal dynamics of relative hydrocarbon composition (%) in the *B. braunii* Ayamè strain (Race B).

Hydrocarbons	Retention Time (min)	Relative Quantity (%) on Each Sampling Day								
		0	3	6	12	18	24	30	36	42
C_{33}	16.029	5.74 ± 0.21 ^{a}	6.12 ± 0.15 ^{a}	5.97 ± 0.20 ^{a}	5.68 ± 0.19 ^{a}	6.01 ± 0.22 ^{a}	5.79 ± 0.30 ^{a}	5.54 ± 0.48 ^{a}	5.10 ± 0.36 ^{a}	5.83 ± 0.21 ^{a}
C_{34a}	16.086	8.31 ± 0.32 ^{a}	8.57 ± 0.35 ^{a}	7.78 ± 0.29 ^{a}	8.73 ± 0.46 ^{a}	9.52 ± 0.41 ^{a}	7.18 ± 0.28 ^{b}	7.94 ± 0.51 ^{ab}	7.71 ± 0.29 ^{ab}	7.11 ± 0.17 ^{b}
C_{34b}	16.162	34.43 ± 0.95 ^{a}	34.06 ± 0.81 ^{a}	34.58 ± 0.93 ^{a}	34.99 ± 0.78 ^{a}	32.47 ± 0.88 ^{ab}	29.35 ± 0.79 ^{bc}	28.15 ± 0.85 ^{c}	28.01 ± 0.44 ^{c}	28.02 ± 0.56 ^{c}
C_{34c}	16.169	9.28 ± 0.38 ^{a}	9.02 ± 0.66 ^{a}	9.03 ± 0.25 ^{a}	7.28 ± 0.78 ^{b}	8.69 ± 0.84 ^{ab}	6.36 ± 0.14 ^{bc}	6.02 ± 0.42 ^{c}	4.39 ± 0.15 ^{d}	4.99 ± 0.38 ^{cd}
C_{34d}	16.279	42.24 ± 1.12 ^{a}	42.23 ± 1.20 ^{a}	42.64 ± 1.45 ^{a}	43.32 ± 1.18 ^{a}	43.31 ± 1.16 ^{a}	51.32 ± 1.35 ^{b}	52.35 ± 1.58 ^{b}	54.79 ± 1.45 ^{c}	54.05 ± 1.22 ^{bc}

Note: Values are expressed as mean ± standard deviation (n = 3). Different lowercase superscript letters (a, b, c, d) within the same row indicate statistically significant differences among sampling days for a given hydrocarbon fraction ($p \leq 0.05$). Subscripts a, b, c, and d represent isomers of the C_{34} hydrocarbon with different retention times.

Hydrocarbons in the Madras 3 strain representing Race L exhibited a uniform structural pattern, consisting predominantly of a C_{40} chain length throughout the entire 42-day duration (Table 4). Three specific isomers (C_{40a}, C_{40b}, and C_{40c}) were consistently detected. Unlike the UTEX 572 and Ayamè strains, the isomeric distribution in Madras 3 demonstrated temporal stability, with the dominant C_{40b} isomer constantly maintaining a relative abundance of approximately 70.3% to 72.4% within all defined growth phases.

Table 4. Temporal dynamics of relative hydrocarbon composition (%) in the *B. braunii* Madras 3 strain (Race L).

Hydrocarbon	Retention Time (min)	Relative Quantity (%) on Each Sampling Day								
		0	3	6	12	18	24	30	36	42
C_{40a}	19.587	18.56 ± 0.62 ^{a}	19.78 ± 0.68 ^{a}	18.94 ± 0.65 ^{a}	19.36 ± 0.66 ^{a}	19.95 ± 0.70 ^{a}	18.58 ± 0.59 ^{a}	18.56 ± 0.77 ^{a}	20.02 ± 0.47 ^{a}	19.52 ± 0.67 ^{a}
C_{40b}	19.706	72.38 ± 1.85 ^{a}	70.35 ± 1.78 ^{a}	71.78 ± 1.82 ^{a}	71.48 ± 1.80 ^{a}	70.65 ± 1.76 ^{a}	72.30 ± 1.59 ^{a}	72.17 ± 1.28 ^{a}	70.56 ± 1.55 ^{a}	71.47 ± 1.39 ^{a}
C_{40c}	19.755	9.06 ± 0.35 ^{a}	9.87 ± 0.39 ^{a}	9.28 ± 0.36 ^{a}	9.16 ± 0.31 ^{a}	9.40 ± 0.37 ^{a}	9.12 ± 0.29 ^{a}	9.27 ± 0.51 ^{a}	9.42 ± 061 ^{a}	9.01 ± 0.42 ^{a}

Note: Values are expressed as mean ± standard deviation (n = 3). The absence of superscript letters within rows indicates no statistically significant differences across sampling days ($p > 0.05$). Subscripts a, b, and c represent isomers of the C_{40} hydrocarbon with different retention times.

4. Discussion

4.1. Effects of Algal Growth Phase on Hydrocarbon Content

The three strains of *B. braunii* exhibited divergent kinetic patterns in growth and hydrocarbon dynamics between the exponential and stationary phases. A common physiological trend observed was that hydrocarbons accumulated predominantly during active growth and continued to increase into the stationary phase [30]. This aligns with findings from Lv et al. [31] and Mansour et al. [20], who noted that lipid and hydrocarbon fractions in various microalgae often increase in the stationary phase due to the progressive metabolic channelling of fixed carbon into storage reserves when cell division slows down. However, temporal tracking in this study revealed a critical strain-specific divergence during late cultivation.

For the UTEX 572 strain, the overall cellular and matrix-associated hydrocarbon content peaked on day 12 during the exponential phase and subsequently decreased as the culture entered the decline phase on day 30. Considering that *B. braunii* uniquely sequesters the vast majority of its synthesized hydrocarbons within a complex extracellular matrix rather than intracellular lipid bodies, attributing this loss to endogenous hydrocarbon catabolism remains mechanistically unsupported, as enzymatic evidence for the internal degradation of these extensive extracellular polymers is fundamentally lacking. Instead, this apparent reduction in hydrocarbon percentage on a dry weight basis is proposed as a plausible working hypothesis driven by a combination of physiological denominator inflation and matrix-handling artifacts inherent to aging batch cultures [32]. Specifically, as cell viability drops and cultures enter the decline phase, widespread cell autolysis releases substantial amounts of intracellular organic compounds, including proteins, carbohydrates, and non-hydrocarbon metabolites, that contribute to the total dry weight. This metabolic shift inflates the dry biomass denominator, thereby depressing the calculated hydrocarbon percentage on a dry weight basis without necessarily reflecting a true net loss of absolute hydrocarbon mass. Furthermore, the progressive deterioration of colonial integrity in aging

cultures leads to the spatial dissociation of the dispersed, hydrocarbon-rich extracellular matrix, which may escape standard membrane filtration or be inadequately recovered during gravimetric quantification. While this working hypothesis aligns with bioprocess theory, direct confirmation requires future empirical validation through rigorous volumetric mass balance quantification on a continuous per liter basis paired with single-cell viability assays to definitively resolve matrix detachment kinetics from metabolic shifts. Given the well-documented chemical recalcitrance of *B. braunii* biopolymers, which underpins their geological persistence in petroleum formation, hypotheses relying on rapid heterotrophic bacterial degradation remain speculative in the absence of dedicated microbiome sequencing and should be interpreted with caution.

Conversely, Ayamè and Madras 3 maintained stable stationary biomass without an overt decline phase, allowing for sustained hydrocarbon accumulation. Interestingly, the physiological trade-off between growth and lipid synthesis varied markedly among the races [33]. Sicko-Goad and Andresen [34] reported that high lipid accumulation in diatoms is frequently inversely correlated with population growth rates. In this study, this inverse relationship was observed in the Ayamè strain, where substantial hydrocarbon accumulation coincided with a sluggish growth rate. This metabolic state typically arises when photosynthetic energy input surpasses the cellular capacity for macromolecular biosynthesis and division, shunting excess reducing equivalents and carbon skeletons into neutral lipid or hydrocarbon reservoirs [35]. However, the UTEX 572 strain diverged from this conventional pattern by combining a high specific growth rate with high exponential hydrocarbon productivity. These contrasting physiological behaviors dictate that harvest timing cannot be generalized; while hydrocarbon harvesting for slow-growing, high-content strains like Ayamè is optimal upon entry into the stationary phase, fast-growing strains like UTEX 572 must be harvested promptly at the termination of the exponential phase to prevent biomass and yield degradation.

It should be emphasized that the static batch system utilized in this study, involving manual agitation twice daily without direct carbon dioxide supplementation, represents a standardized low-shear baseline condition designed to evaluate inherent physiological kinetics while preserving extracellular colony integrity. However, given that *B. braunii* forms highly buoyant, hydrocarbon-rich aggregate colonies susceptible to self-shading and localized carbon depletion, this intermittent agitation likely restricted gas-liquid mass transfer and light attenuation within the culture vessel. Consequently, such passive carbon supply and light restriction may have imposed an additional environmental barrier that extended the initial lag phase, particularly for tropical or geographically specialized isolates like Ayamè and Madras 3 [13]. Future process scaling must incorporate continuous active aeration and dynamic mixing to eliminate gas transfer bottlenecks and optimize volumetric productivity.

4.2. Variations of Hydrocarbon Signatures in Different Growth Phases

Microbial lipid composition is widely recognized to fluctuate in response to environmental and developmental shifts in batch cultures [36–38]. Nevertheless, the present study demonstrated that the homologous series distributions and dominant carbon chain lengths of each *B. braunii* strain remained stable throughout all growth phases [39]. As corroborated by representative chromatographic profiles, this chemical stability corroborates the observations of Mansour et al. [20] and previous bacterial studies [40], which reported invariant fatty acid and sterol signatures throughout a batch growth cycle.

Although the predominant chemical structures were conserved, subtle quantitative shifts in isomeric distribution were detected. While Villarreal-Rosales et al. [41] noted moderate shifts in C_{27} proportions during growth phases in *B. braunii*, detailed temporal tracking revealed that the primary isomer C_{29a} in the UTEX 572 increased from 36.0% to 41.5%, and C_{34d} in the Ayamè increased from 43.3% to 54.8% over time. By precisely aligning these temporal isomeric fluctuations with the respective growth trajectories, a strong correlation emerges between isomeric shifting and developmental phase transitions. Specifically, the significant accumulation of dominant isomers (such as C_{29a} and C_{34d}) coincides synchronously with the deceleration of specific growth rates and the cultures' entry into the stationary or decline phases. This temporal alignment indicates that such targeted isomeric redistributions are not merely random metabolic drift, but likely serve as biochemical indicators of critical environmental thresholds, such as the exhaustion of macronutrients (e.g., nitrogen or phosphorus) in the batch medium. Furthermore, considering that *B. braunii* uniquely sequesters its synthesized hydrocarbons within a complex extracellular matrix, this isomeric shift presents relevant physiological implications. Modifying the internal ratios of specific structural isomers under nutrient-depleted stress conditions may constitute an active adaptive mechanism. This localized chemical restructuring could physically modulate the viscosity, hydrophobicity, and overall fluidity of the secreted hydrocarbon pool, thereby preserving the structural integrity and protective barrier function of the colony's extracellular matrix when primary cellular proliferation ceases [42].

Despite these phase-dependent and physiologically adaptive isomeric redistributions, the overarching biochemical fingerprints (e.g., C_{29}/C_{31} for Race A, C_{34} for Race B, and C_{40} for Race L) remained conserved. From a bioprocess engineering perspective, this chemical robustness is advantageous, indicating that industrial harvesting can be scheduled flexibly at various growth stages without compromising the intrinsic quality or downstream catalytic utility of the extracted hydrocarbon feedstock.

4.3. Algal Strain Selection for Biofuel Production

Biofuel commercialization from microalgae is fundamentally governed by the techno-economic trade-off between biomass productivity and intracellular lipid or extracellular hydrocarbon content [43]. A longstanding bottleneck in strain selection is that strains exhibiting high lipid content frequently suffer from inferior growth kinetics [44]. The comparative evaluation of the three *B. braunii* strains herein provides empirical support for this physiological dilemma while offering tailored pathways for industrial application.

However, as underscored throughout this study, it is necessary to address the experimental bias and methodological limitations inherent in utilizing a single, uniform culture regime (specifically Bold-3N medium at 24 °C) across strains originating from vastly different aquatic ecosystems and geographic backgrounds. The extended 12-day lag phase and delayed active growth observed in the Ayamè (Race B, isolated from African freshwater habitats) and Madras 3 (Race L, Indian origin) strains do not provide definitive evidence of an inherent metabolic sluggishness or a permanent low-productivity phenotype. Instead, this pronounced lag strongly indicates that the standardized Bold-3N formulation and thermal setting were sub-optimal for their specific physiological and metabolic requirements. This creates an inadvertent experimental bias that favors the UTEX 572 strain, which appears coincidentally better adapted to these baseline conditions. Microalgal chemical races of *B. braunii* exhibit substantial ecological and physiological divergence, and thus categorizing Ayamè and Madras 3 as intrinsically slow-cycling is a physiological oversimplification. Their protracted growth trajectories are artifactual reflections of nutritional or environmental sub-optimality imposed by the current experimental protocol.

Despite these methodological caveats, evaluating performance under the current baseline reveals clear industrial trade-offs. Although the UTEX 572 strain (Race A) possessed a moderate hydrocarbon content (16.8%), its superior specific growth rate (0.168 ± 0.008 day^{-1}) and peak hydrocarbon productivity (0.029 ± 0.001 g L^{-1} day^{-1}) establish it as the most viable candidate for large-scale short-cycle biofuel production among the tested organisms. As emphasized by previous screening frameworks, volumetric productivity during the exponential phase serves as the most reliable metric for industrial strain prioritization [45]. In contrast, while the Ayamè strain (Race B) yielded the highest absolute hydrocarbon content (27.2%), its protracted acclimation period, slow growth rate (0.076 ± 0.002 day^{-1}), and moderate productivity position it as a secondary candidate, better suited for extended-batch or semi-continuous cultivation systems with prolonged solid retention times. Madras 3 (Race L), constrained by minimal productivity and low accumulation, remains economically unviable for standalone hydrocarbon extraction under these parameters.

Furthermore, the present experimental observations demonstrate that strain selection must factor in temporal dynamics alongside absolute yields, as UTEX 572 rapidly completed its growth cycle within 12 days, whereas Ayamè and Madras 3 required 30 days to reach comparable developmental milestones. While environmental factors such as seasonal shifts can alter algal lipid profiles in outdoor open systems, intrinsic strain-specific kinetics dictate baseline operational parameters under defined regimes. Ultimately, overcoming the productivity-content dilemma requires moving beyond rigid, undifferentiated cultivation strategies. Future bioprocess development must prioritize tailoring race-specific nutritional matrices, such as custom nitrogen-to-phosphorus ratios, specialized trace metal or vitamin supplements, and salinity adjustments, to unlock the true physiological potential of slow-cycling or high-accumulation strains like Ayamè [46]. By doing so, operators can judiciously match fast-cycling strains like UTEX 572 for high-turnover volumetric output, while unlocking the maximum extraction capacity of high-accumulation strains under optimized, customized cultivation frameworks.

5. Conclusions

This comparative evaluation of *Botryococcus braunii* strains UTEX 572 representing Race A, Ayamè representing Race B, and Madras 3 representing Race L defines the growth kinetics, hydrocarbon accumulation patterns, and isomeric distributions over a 42-day cultivation period. The data demonstrate marked physiological divergences among the evaluated strains rather than universally within the chemical races. Under the specific standardized cultivation conditions applied in this study, UTEX 572 exhibited rapid growth and achieved its peak hydrocarbon productivity during a compressed exponential phase, reaching a maximum yield of 0.303 g L^{-1} on day 18. In contrast, constrained by the uniform baseline settings, specifically Bold-3N medium at 24 °C, Ayamè required

a longer cultivation cycle for initial acclimation but accumulated the highest absolute hydrocarbon content of 27.2% and a volumetric yield of 0.466 g L^{-1} upon entering the stationary phase. Madras 3 displayed lower overall biomass and hydrocarbon yield throughout the cultivation period under these specific experimental constraints.

Chemical profile analyses revealed that the homologous series distributions of each race remained consistent across growth phases. Although minor quantitative shifts occurred within internal isomeric fractions, the predominant hydrocarbon structures did not vary significantly, indicating that harvest timing within the tested window does not disrupt the fundamental chemical identity of the extracted feedstock. Crucially, the observed kinetic behaviors, including the extended lag phases in Ayamè and Madras 3, reflect strain-specific performance governed strictly by the current experimental framework rather than defining absolute biological boundaries. Consequently, these findings should not be interpreted as definitive limits for commercial deployment. While UTEX 572 proves advantageous for rapid volumetric turnover under the present batch framework, transitioning to dynamic photobioreactors, continuous culture systems, or race-specific nutrient formulations may significantly reconfigure these observed performance hierarchies. Therefore, industrial strain selection requires flexible, system-specific process optimization rather than reliance on static baseline phenotypes.

Supplementary Materials

The additional data and information can be downloaded at: https://media.sciltp.com/articles/others/26111211 27474935/ALE-26090059-SI.pdf. Figure S1: Representative gas chromatography-mass spectrometry (GC-MS) chromatograms of hydrocarbon extracts from three *Botryococcus braunii* chemical races: (**top**) UTEX 572 (Race A), displaying characteristic C_{25}–C_{31} fractions with primary peaks at retention times (R_t) of 17.687 min and 18.335 min; (**middle**) Ayamè (Race B), displaying C_{33}–C_{34} fractions dominated by the C_{34d} peak at R_t = 16.279 min; and (**bottom**) Madras 3 (Race L), displaying the C_{40} fraction dominated by the C_{40b} peak at R_t = 19.706 min. The chromatograms illustrate characteristic retention time separations and unique elution profiles among the evaluated strains under standardized analytical parameters.

Author Contributions

H.X.: Data curation, formal analysis, visualization. L.S.: Conceptualization, methodology, investigation, data curation, writing—original draft, review & editing, supervision. All authors have read and agreed to the published version of the manuscript.

Funding

This research was funded by Flinders University and SQC Pty Ltd. The APC was funded by the funding sources mentioned above.

Institutional Review Board Statement

Not applicable.

Informed Consent Statement

Not applicable.

Data Availability Statement

The datasets generated and analyzed during the current study are available from the corresponding author upon reasonable request.

Acknowledgments

We express our sincere appreciation to Daniel Jardine from Flinders Analytical for his expert guidance and technical assistance with the GC/GC-MS analyses.

Conflicts of Interest

The authors declare no conflict of interest.

Use of AI and AI-Assisted Technologies

During the preparation of this work, the authors used Grammarly (cloud-based web application and browser extension, accessed in early-to-mid October 2026) for language editing and grammar improvement. After using this tool, the authors reviewed and edited the content as needed and take full responsibility for the published article.

References

1. Rial, R.C. Biofuels Versus Climate Change: Exploring Potentials and Challenges in the Energy Transition. *Renew. Sustain. Energy Rev.* **2024**, *196*, 114369. https://doi.org/10.1016/j.rser.2024.114369.
2. Wirawan, S.S.; Solikhah, M.D.; Setiapraja, H.; et al. Biodiesel Implementation in Indonesia: Experiences and Future Perspectives. *Renew. Sustain. Energy Rev.* **2024**, *189*, 113911. https://doi.org/10.1016/j.rser.2023.113911.
3. Silitonga, A.S.; Riayatsyah, T.M.I.; Kalam, M.A.; et al. Status, Developments, and Sustainability of Biowaste Feedstock: A Review of Current Progress. *Renew. Sustain. Energy Rev.* **2025**, *217*, 115769. https://doi.org/10.1016/j.rser.2025.115769. Correction in *Renew. Sustain. Energy Rev.* **2025**, *219*, 115862. https://doi.org/10.1016/j.rser.2025.115862.
4. Prajapati, A.K.; Mahajan, A.; Jadhav, S.M.; et al. Fourth-Generation (4G) Biodiesel: Paving the Way for a Greener and Sustainable Energy Future in Emerging Economies. *Renew. Sustain. Energy Rev.* **2026**, *225*, 116103. https://doi.org/10.1016/j.rser.2025.116103.
5. Ashokkumar, V.; Flora, G.; Kumar, G.; et al. Cutting-Edge Advances in Alga *Botryococcus* for Eco-Friendly Biofuels and High-Value Bioproducts—A Critical Review. *Algal Res.* **2024**, *83*, 103676. https://doi.org/10.1016/j.algal.2024.103676.
6. Ennaceri, H.; Nwoba, E.G.; Ogbonna, C.N.; et al. Progress of Non-Destructive Hydrocarbon Extraction Technology of *Botryococcus braunii*. *Algal Res.* **2023**, *73*, 103156. https://doi.org/10.1016/j.algal.2023.103156.
7. Miyazaki, T.; Furuhashi, K.; Okada, S.; et al. Simultaneous Culture and Hydrocarbon Recovery from *Botryococcus braunii* with Squalane as a Solvent. *J. Appl. Phycol.* **2025**, *37*, 3955–3964. https://doi.org/10.1007/s10811-025-03693-9.
8. Mkpuma, V.O.; Ishika, T.; Moheimani, N.R.; et al. The Potential of Coupling Wastewater Treatment with Hydrocarbon Production Using *Botryococcus braunii*. *Algal Res.* **2023**, *74*, 103214. https://doi.org/10.1016/j.algal.2023.103214.
9. Yu, B.; Gong, P.; Zhang, H.; et al. Evaluation of the Growth, Lipid, and Hydrocarbon Accumulation Abilities in Five Strains of *Botryococcus braunii* (races A, B, and L) (Trebouxiophyceae, Chlorophyta). *Algal Res.* **2025**, *85*, 103809. https://doi.org/10.1016/j.algal.2024.103809.
10. Kleinert, C.; Griehl, C. Identification of Suitable *Botryococcus braunii* Strains for Non-Destructive *In Situ* Hydrocarbon Extraction. *J. Appl. Phycol.* **2021**, *33*, 785–798. https://doi.org/10.1007/s10811-020-02342-7.
11. Yang, S.; Wang, J.; Cong, W.; et al. Utilization of Nitrite as a Nitrogen Source by *Botryococcus braunii*. *Biotechnol. Lett.* **2004**, *26*, 239–243. https://doi.org/10.1023/b:bile.0000013722.45527.18.
12. Biondi, N.; Rodolfi, L.; Tredici, M.R. *Botryococcus braunii* Strain Showa in Annular Photobioreactors under Artificial Light. *J. Appl. Phycol.* **2026**, *in press*. https://doi.org/10.1007/s10811-026-03977-8.
13. Kemel, S.; Marchal, L.; Habiba, W.N.; et al. Investigation of the Colony Size Effect on Light Access and Growth of the Colonial Microalga *Botryococcus braunii* in Photobioreactor. *Algal Res.* **2025**, *90*, 104176. https://doi.org/10.1016/j.algal.2025.104176.
14. Griehl, C.; Kleinert, C.; Griehl, C.; et al. Design of a Continuous Milking Bioreactor for Non-Destructive Hydrocarbon Extraction from *Botryococcus braunii*. *J. Appl. Phycol.* **2015**, *27*, 1833–1843. https://doi.org/10.1007/s10811-014-0472-6.
15. Tasić, M.B.; Pinto, L.F.R.; Klein, B.C.; et al. *Botryococcus braunii* for Biodiesel Production. *Renew. Sustain. Energy Rev.* **2016**, *64*, 260–270. https://doi.org/10.1016/j.rser.2016.06.009.
16. Arbeláez Pérez, A.A.; Calderón, N.D.G.; Montoya, L.M.M.; et al. Photosynthetic Distribution Inside a Cylindrical Photobioreactor for *Botryococcus braunii*: A Fed-Batch Culture Application. *Algal Res.* **2024**, *82*, 103678. https://doi.org/10.1016/j.algal.2024.103678.
17. Patel, A.; Rantzos, C.; Krikigianni, E.; et al. A Bioprocess Engineering Approach for the Production of Hydrocarbons and Fatty Acids from Green Microalga under High Cobalt Concentration as the Feedstock of High-Grade Biofuels. *Biotechnol. Biofuels Bioprod.* **2024**, *17*, 64. https://doi.org/10.1186/s13068-024-02512-6.
18. Baldisserotto, C.; Sabia, A.; Guerrini, A.; et al. Mixotrophic Cultivation of *Thalassiosira pseudonana* with Pure and Crude Glycerol: Impact on Lipid Profile. *Algal Res.* **2021**, *54*, 102194. https://doi.org/10.1016/j.algal.2021.102194.
19. Ganga, R.S.; Korath, A.; Anandan, R.; et al. Variations in Lipid Profile of *Isochrysis galbana*, a Marine Microalga, Grown in Different Culture Media for Their Use as Live Feed in Mariculture. *J. Mar. Biol. Assoc. India* **2023**, *65*, 30–36. https://doi.org/10.6024/jmbai.2023.65.1.2268-03.
20. Mansour, M.P.; Volkman, J.K.; Blackburn, S.I. The Effect of Growth Phase on the Lipid Class, Fatty Acid and Sterol Composition in the Marine Dinoflagellate, *Gymnodinium* sp. in Batch Culture. *Phytochemistry* **2003**, *63*, 145–153. https://doi.org/10.1016/s0031-9422(03)00052-9.

21. Roleda, M.Y.; Slocombe, S.P.; Leakey, R.J.G.; et al. Effects of Temperature and Nutrient Regimes on Biomass and Lipid Production by Six Oleaginous Microalgae in Batch Culture Employing a Two-Phase Cultivation Strategy. *Bioresour. Technol.* **2013**, *129*, 439–449. https://doi.org/10.1016/j.biortech.2012.11.043.
22. Covell, L.; Machado, M.; Vaz, M.G.M.V.; et al. Differential Metabolic Reprogramming Due to Nitrogen Starvation Leads to Remobilization of Storage Metabolites in Microalgal Strains. *J. Biotechnol.* **2026**, *409*, 231–246. https://doi.org/10.1016/j.jbiotec.2025.11.008.
23. Singh, Y. Photosynthetic Activity, and Lipid and Hydrocarbon Production by Alginate-Immobilized Cells of *Botryococcus* in Relation to Growth Phase. *J. Microbiol. Biotechnol.* **2003**, *13*, 687–691.
24. Kawamura, K.; Nishikawa, S.; Hirano, K.; et al. BoCAPS: Rapid Screening of Chemical Races in *Botryococcus braunii* with Direct PCR-CAPS. *Algal Res.* **2022**, *66*, 102789. https://doi.org/10.1016/j.algal.2022.102789.
25. Mohamadnia, S.; Valverde-Pérez, B.; Tavakoli, O.; et al. Progress and Prospects in Metabolic Engineering Approaches for Isoprenoid Biosynthesis in Microalgae. *Biotechnol. Biofuels Bioprod.* **2025**, *18*, 64. https://doi.org/10.1186/s13068-025-02665-y.
26. Abdelmagid, A.M.; Glushkov, D.O.; Sviridenko, A.S.; et al. Sustainable Aviation Fuels: A Review of Atomization, Combustion and Emission Characteristics. *Biotechnol. Biofuels Bioprod.* **2026**, *19*, 52. https://doi.org/10.1186/s13068-026-02777-z.
27. Okada, S.; Murakami, M.; Yamaguchi, K. Hydrocarbon Composition of Newly Isolated Strains of the Green Microalga *Botryococcus braunii*. *J. Appl. Phycol.* **1995**, *7*, 555–559. https://doi.org/10.1007/bf00003942.
28. Levasseur, M.; Thompson, P.A.; Harrison, P.J. Physiological Acclimation of Marine Phytoplankton to Different Nitrogen Sources. *J. Phycol.* **1993**, *29*, 587–595. https://doi.org/10.1111/j.0022-3646.1993.00587.x.
29. Casadevall, E.; Dif, D.; Largeau, C.; et al. Studies on Batch and Continuous Cultures of *Botryococcus braunii*: Hydrocarbon Production in Relation to Physiological State, Cell Ultrastructure, and Phosphate Nutrition. *Biotechnol. Bioeng.* **1985**, *27*, 286–295. https://doi.org/10.1002/bit.260270312.
30. Rani, S.; Senapati, V.; Senapati, V.; et al. Assessment of Growth Dynamics, Metabolite Production Phasic Analysis in Microalgae *Scenedesmus rotundus* under Varying pH Conditions. *Bioresour. Technol.* **2026**, *441*, 133533. https://doi.org/10.1016/j.biortech.2025.133533.
31. Lv, X.; Zou, L.; Sun, B.; et al. Variations in Lipid Yields and Compositions of Marine Microalgae during Cell Growth and Respiration, and Within Intracellular Structures. *J. Exp. Mar. Biol. Ecol.* **2010**, *391*, 73–83. https://doi.org/10.1016/j.jembe.2010.06.010.
32. Ren, T.; Zhou, Y.; Cui, X.; et al. Differentiation and Quantification of Extracellular Polymeric Substances from Microalgae and Bacteria in the Mixed Culture. *Water Res.* **2024**, *256*, 121641. https://doi.org/10.1016/j.watres.2024.121641.
33. Zhang, H.; Tan, Y.; Zhu, R.; et al. Red Light Trade-Off Regulating the Negative Effects of Nitrogen Concentration to Improve Lipid and Astaxanthin Production in the Filamentous Green Microalga *Oedocladium carolinianum*. *Algal Res.* **2024**, *80*, 103510. https://doi.org/10.1016/j.algal.2024.103510.
34. Sicko-Goad, L.; Andresen, N.A. Effect of Growth and Light/Dark Cycles on Diatom Lipid Content and Composition. *J. Phycol.* **1991**, *27*, 710–718. https://doi.org/10.1111/j.0022-3646.1991.00710.x.
35. Xu, Z.; Qi, J.; Wang, S.; et al. Algal Cell Bionics as a Step towards Photosynthesis-Independent Hydrogen Production. *Nat. Commun.* **2023**, *14*, 1872. https://doi.org/10.1038/s41467-023-37608-4.
36. Das, S.; Das, S.; Ghangrekar, M.M. Enzymatic Cell Disruption followed by Application of Imposed Potential for Enhanced Lipid Extraction from Wet Algal Biomass Employing Photosynthetic Microbial Fuel Cell. *Bioresour. Technol.* **2022**, *363*, 127924. https://doi.org/10.1016/j.biortech.2022.127924.
37. Khandelwal, A.; Vijay, A.; Dixit, A.; et al. Microbial Fuel Cell Powered by Lipid Extracted Algae: A Promising System for Algal Lipids and Power Generation. *Bioresour. Technol.* **2018**, *247*, 520–527. https://doi.org/10.1016/j.biortech.2017.09.119.
38. Rikta, S.Y.; Sraboni, H.J.; Rahman, E. Surface-Active Agents for the Disruption of Algal Cell Walls: An Alternative for Lipid Extraction. In *Algal Bioreactors: Science, Engineering and Technology of Downstream Processes*; Elsevier: Amsterdam, The Netherlands, 2025; Vol. 2, pp. 215–232. https://doi.org/10.1016/b978-0-443-14059-4.00020-9.
39. Liao, J.; Feng, Q.; Lu, H.; et al. n-C27 Predominance and 13C Enrichment by Bicarbonate Assimilation of Race A of *Botryococcus braunii* in Chinese Maoming Oilshales. *Chem. Geol.* **2022**, *602*, 120905. https://doi.org/10.1016/j.chemgeo.2022.120905.
40. Syakti, A.D.; Mazzella, N.; Torre, F.; et al. Influence of Growth Phase on the Phospholipidic Fatty Acid Composition of Two Marine Bacterial Strains in Pure and Mixed Cultures. *Res. Microbiol.* **2006**, *157*, 479–486. https://doi.org/10.1016/j.resmic.2005.11.001.
41. Villarreal-Rosales, E.; Metzger, P.; Casadevall, E. Ether Lipid Production in Relation to Growth in *Botryococcus braunii*. *Phytochemistry* **1992**, *31*, 3021–3027. https://doi.org/10.1016/0031-9422(92)83439-6.
42. Kurpan, D.; Ciardi, M.; Pessôa, L.; et al. Impacts of Harvesting Methods and Medium Recycling on Rheology and Composition of Recycled Medium and Cell Concentrates of *Limnospira platensis* Semi-Continuous Cultures. *J. Environ. Chem. Eng.* **2025**, *13*, 119570. https://doi.org/10.1016/j.jece.2025.119570.

43. Rodolfi, L.; Chini Zittelli, G.; Bassi, N.; et al. Microalgae for Oil: Strain Selection, Induction of Lipid Synthesis and Outdoor Mass Cultivation in a Low-Cost Photobioreactor. *Biotechnol. Bioeng.* **2009**, *102*, 100–112. https://doi.org/10.1002/bit.22033.
44. Rosenberg, J.N.; Oyler, G.A.; Wilkinson, L.; et al. A Green Light for Engineered Algae: Redirecting Metabolism to Fuel a Biotechnology Revolution. *Curr. Opin. Biotechnol.* **2008**, *19*, 430–436. https://doi.org/10.1016/j.copbio.2008.07.008.
45. Camstra, J.S.; van Mierlo, P.; Trincheiras, I.; et al. Freshwater Microalgae Strain Selection for Industrial Triacylglycerol Production—A Scale-Down Approach. *Algal Res.* **2026**, *97*, 104788. https://doi.org/10.1016/j.algal.2026.104788.
46. Gao, L.; Ding, W.; Xi, J.; et al. Effects of Different Nitrogen/Phosphorus Ratios on the Growth and Metabolism of Microalgae *Scenedesmus obliquus* Cultured in the Mixed Wastewater from Primary Settling Tank and Sludge Thickener. *Process Saf. Environ. Prot.* **2023**, *170*, 824–833. https://doi.org/10.1016/j.psep.2022.12.059.